



## Severe late Miocene droughts affected western Eurasia

Geanina A. Butiseacă<sup>a,b,\*</sup>, Iuliana Vasiliev<sup>a</sup>, Marcel T.J. van der Meer<sup>c</sup>, Wout Krijgsman<sup>d</sup>, Dan V. Palcu<sup>d,e</sup>, Angelica Feurdean<sup>f</sup>, Eva M. Niedermeyer<sup>a</sup>, Andreas Mulch<sup>a,b</sup>

<sup>a</sup> Senckenberg Biodiversity and Climate Research Centre (SBIK-F), Senckenberganlage 25, D-60325 Frankfurt am Main, Germany

<sup>b</sup> Institute of Geosciences, Goethe University Frankfurt, Altenhöferallee 1, 60438 Frankfurt am Main, Germany

<sup>c</sup> Royal Netherlands Institute for Sea Research, Department of Marine Microbiology and Biogeochemistry, P.O. Box 59, 1790 AB Den Burg, Texel, the Netherlands

<sup>d</sup> Fort Hoofddijk, Paleomagnetic Laboratory, Utrecht University, Budapestlaan17, 3584 CD, Utrecht, the Netherlands

<sup>e</sup> Instituto Oceanográfico da Universidade de São Paulo Praça do Oceanográfico, 191, 05508-120 São Paulo-SP, Brazil

<sup>f</sup> Department of Physical Geography, Goethe University, Altenhöferallee 1, 60438 Frankfurt am Main, Germany

### ARTICLE INFO

Guest Editor: Fabienne Marret-Davies.

#### Keywords:

Paratethys isolation  
Late Miocene droughts  
Vegetation shift  
Biomarkers  
Isotope geochemistry

### ABSTRACT

A large and highly dynamic aquatic system called Paratethys governed important elements of the middle and late Miocene (15.97–5.33 Ma) hydrology in western Eurasia. So far, the impact of the vast Paratethys water body on the Eurasian climate, however, is not yet understood. Here we apply biomarker analyses coupled to compound-specific hydrogen and carbon isotope data to track changes in sea surface temperature, mean annual air temperature, hydrological budget and vegetation changes to reconstruct long-term western Eurasian climate conditions between 12.7 and 7.65 Ma in the Black Sea region. Biomarker data from Panagia (Russia) indicate the presence of three exceptionally evaporative intervals peaking at 9.65, 9.4 and 7.9 Ma. These peaks in evaporation relate to aridity, parallel increasing fire activity and are associated with changes in vegetation. Carbon isotope and pollen data support the evidence of an increase in C<sub>4</sub> plants associated with these dry intervals. At 9.66 Ma, alkenone producing algae appear in the basin and thrive for the subsequent two million years. Cumulative fluctuations in both hydrology and surface temperature of Paratethys might have enhanced rainfall seasonality in western Eurasia as a response to changes in evaporation over the Paratethys basin. Our combined data suggest a strong regional imprint on overall climate patterns, dominated by basin dynamics causing Paratethys volume and surface reduction. Collectively, the presented biomarker results provide evidence of severe droughts affecting the late Miocene circum-Paratethys region, leading to a direct impact on the evolution of biota in the basin and its surroundings.

### 1. Introduction

The interplay between tectonics, landscape and climate change influenced the middle and late Miocene development of the Eurasian continental interior (Fig. 1). As a result, the Paratethys, a large epicontinental water body, became fragmented into smaller basins during the late Miocene (11.6–5.3 Ma), with temporary or no connection to the global oceans (Popov et al., 2006; Fig. 1). Such semi-isolated water bodies are highly sensitive to changes in their hydrological balance, which is directly reflected in water temperature, salinity, circulation, and therefore oxygenation of the water column. A general lack of age-diagnostic marine biota characterizes the Paratethyan sub-basins, causing difficulties for reliable biostratigraphic correlation to the marine realm. Furthermore, commonly used geochemical methods in

paleoceanography (e.g. stable oxygen and carbon isotopes on foraminifera) are of limited use as the high degree of endemism led to the absence of widespread marine (e.g. planktonic) foraminifera species. As Paratethys water bodies evolved (quasi)disconnected from the global oceans they acquired particular environmental characteristics which can be untangled only through multi-proxy approaches.

Recently established magneto-biostratigraphy provides a reliable geochronological framework for the middle to late Miocene Panagia section of the Eastern Paratethys (Popov et al., 2016; Palcu et al., 2021), a section exposed on the Taman Peninsula (northern Black Sea, Russia; Fig. 1). Here, we investigate the biomarker record of the Panagia section to reconstruct the climatic conditions between 12.7 and 7.65 Ma (Volhynian to Khersonian local stages), with a special focus on the 9.75 to 7.65 Ma (latest Bessarabian to Khersonian) time interval. We use

\* Corresponding author at: Senckenberg Biodiversity and Climate Research Centre (SBIK-F), Senckenberganlage 25, D-60325 Frankfurt am Main, Germany.

E-mail address: [geanina.butiseaca@senckenberg.de](mailto:geanina.butiseaca@senckenberg.de) (G.A. Butiseacă).

<https://doi.org/10.1016/j.gloplacha.2021.103644>

Received 23 June 2021; Received in revised form 12 August 2021; Accepted 7 September 2021

Available online 10 September 2021

0921-8181/© 2021 Elsevier B.V. All rights reserved.

biomarker analyses coupled to compound-specific hydrogen ( $\delta^2\text{H}$ ) and carbon ( $\delta^{13}\text{C}$ ) isotopes to track a complex array of environmental changes. We reconstruct: 1) sea surface temperatures (SSTs) using isoprenoidal glycerol dialkyl tetraethers (isoGDGTs), biomarkers synthesized by Archaea group that reflect the near-surface conditions within the water column; 2) mean annual air temperatures (MAT) based on branched (brGDGTs), biomarkers produced primarily by soil bacteria in the circum-Paratethys region. We further analyze changes in the hydrological budget of the Paratethys basin through: 3)  $\delta^2\text{H}$  values from alkenones (produced by coccolithophoriid algae within the uppermost Paratethys water column) and 4)  $\delta^2\text{H}$  measured on long chain *n*-alkanes (produced by higher terrestrial plants recording precipitation changes in the basin catchment). We monitor: 5) changes in basin productivity through  $\delta^{13}\text{C}$  values of alkenones and reconstruct 6) changes in vegetation surrounding the basin using  $\delta^{13}\text{C}$  values of *n*-alkanes. Biomarker data are finally supplemented by 7) charcoal analysis and coupled to existing palynological data (Razumkova, 2012) to identify changes in paleo-fire activity and paleo-vegetation.

Similar proxy records previously identified two phases of severe droughts in the Black Sea region (around 8 and 5.8 Ma; Vasilev et al., 2013, 2015, 2019). The present work significantly extends these records back in time to 12.7 Ma, identifying major environmental changes in the Eastern Paratethys that affect large parts of Eurasia.

## 2. Stratigraphy of sampled interval and age model

The Panagia section (45°09' N, 36°38' E, Taman Peninsula, Black Sea coast, Russia; Fig. 1) covers a significant part of the late Miocene in the Eastern Paratethys (Popov et al., 2016). Because of protracted endemism in the Paratethys basin, we rely on the regional stratigraphy, with the late Miocene successions divided into the Sarmatian *sensu lato* (*s.l.*) stage with Volhynian, Bessarabian and Khersonian substages and the Maeotian and Pontian stages (Fig. 2). The 638 m thick Panagia section preserves a fairly complete sedimentary record of the 12.7–7.65 Ma interval with Bessarabian and Khersonian substages being exceptionally well exposed (Popov et al., 2016). Magnetostratigraphic dating of the Panagia section pins the base of the Sarmatian (*s.l.*) at 12.65 Ma (at 2 m; Palcu et al., 2017), the Volhynian–Bessarabian transition at ~12 Ma, the Bessarabian–Khersonian boundary at 9.65 Ma (at 310 m) and the

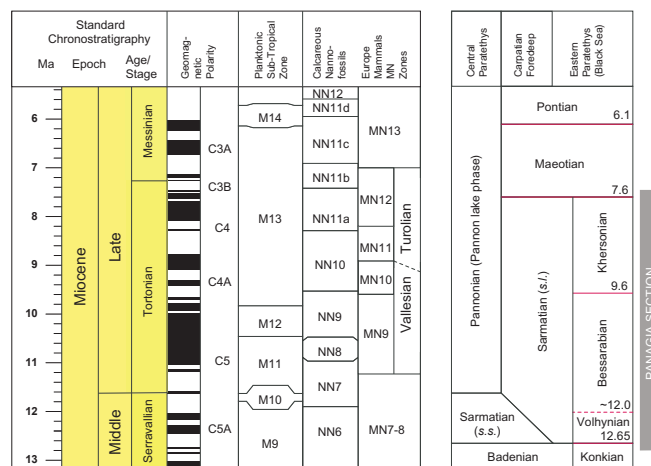


Fig. 2. Chronostratigraphic correlation of the Middle - Late Miocene (Hilgen et al., 2012) to Paratethys regional substages. Geomagnetic polarity time scale with chron nomenclature and biozones are presented (M for planktonic fauna, NN for calcareous nannofossils and MN for European mammal zonations). The grey bar represents the time interval covered by Panagia section.

Khersonian–Maeotian boundary at 7.65 Ma (at 625 m; Palcu et al., 2021; Fig. 2). The poorly-exposed Volhynian consists of alternations of dark clays with sulphur films and thin carbonate layers, while the Bessarabian comprises clays and marls with increasing carbonate intercalations in its terminal part (Popov et al., 2016).

The Khersonian continues with alternations of clays and silty clays, laminated dark shales with yellowish sulphur films, gypsum crystals, pyrite and thin diatomite layers being almost totally devoid of carbonates.

## 3. Material and methods

### 3.1. Organic geochemistry, lipid extraction, fractions separation and analyses

Fifty-seven sedimentary rock samples weighing between 14 and 32 g

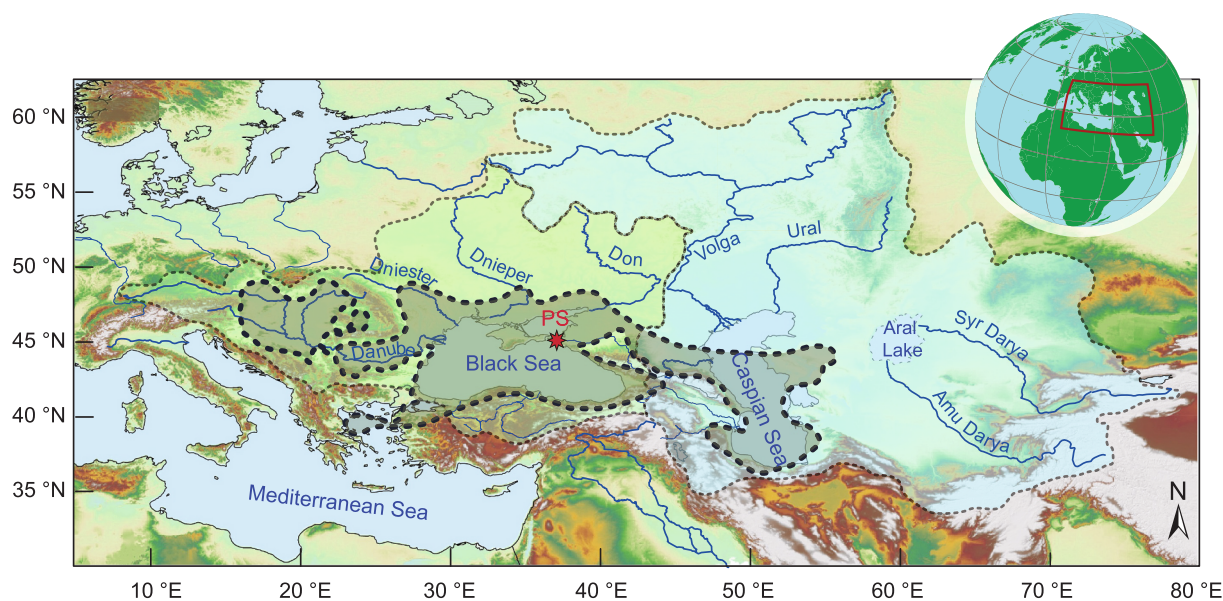


Fig. 1. Map showing the Late Miocene Paratethys domain extension (black dashed line) overlapped onto the present day geographical configuration. The present-day drainage basins (grey dashed contours) of Black and Caspian Seas hint for the areal extent of the Paratethys drainage basin. The Panagia section (PS) is indicated with a red star. (For interpretation of the references to colour in this figure legend, the reader is referred to the web version of this article.)

were analyzed. The complete and detailed workflow for the organic geochemistry is presented in the supplementary material online. In short, the fifty-seven selected samples underwent drying, grinding, total lipid extraction (TLE) and removal of elemental sulphur. Afterwards, a fraction of the TLE was archived. The remainder was then separated using Al<sub>2</sub>O<sub>3</sub> column chromatography into apolar, ketone and polar fractions. The apolar fraction containing *n*-alkanes was purified (using AgNO<sub>3</sub> column, or urea adduction, when needed) and later identified using the Gas Chromatography-Mass Spectrometry (GC-MS) at Senckenberg Biodiversity and Climate Research Centre (SBIK-F) in Frankfurt (see supplementary material). The ketone fraction containing alkenones was occasionally purified using AgNO<sub>3</sub> column and subsequently measured on the GC-MS. The polar fraction containing GDGTs, filtered over a 0.45 mm PTFE filter, was analyzed and quantified at the SBIK-F laboratory using a Shimadzu, UFLC performance HPLC mass spectrometer (see supplementary material).

The SSTs were obtained by using TEX<sub>86</sub> (TetraEther indeX of tetraethers consisting of 86 carbon atoms) values that were calculated according to the definition of Schouten et al. (2002) and converted into SST using the calibration and recommendation of Kim et al. (2010) to apply the TEX<sub>86</sub><sup>H</sup> above 15 °C (i.e. outside the polar and subpolar domains).

The distribution of brGDGTs, expressed as the Methylation index of Branched Tetraethers (MBT) and the Cyclisation ratio of Branched Tetraethers (CBT), displays a significant linear correlation with modern MAT in the range of 6 to 27 °C (Weijers et al., 2007; Peterse et al., 2012; De Jonge et al., 2014). From the multiple existent calibrations, we chose to use Peterse et al. (2012) as a more conservative choice given that the expected environmental changes for the ~5 Myr duration of the studied interval are large. Paleosoil pH estimates use the CBT index based on brGDGTs and follow Peterse et al. (2012).

The δ<sup>2</sup>H was determined by GC/Thermal Conversion (TC)/ isotope monitoring MS (irMS) using an Agilent GC coupled to a Thermo Electron DELTA Plus XL mass spectrometer, via a ConFlo IV. Alkane and alkenone fractions were injected on column at the Royal Netherlands Institute for Sea Research (NIOZ) (see supplementary material). The carbon isotope ratios (δ<sup>13</sup>C) of individual *n*-alkanes and alkenones were measured on the purified and adducted apolar and alkenone fractions on the GC-irMS using similar conditions as for δ<sup>2</sup>H measurements at NIOZ.

### 3.2. Charcoal preparation and quantification

To evaluate past biomass burning in the region, charcoal particles were extracted from fifty-eight samples, in compliance with the organic geochemistry sampling (see supplementary material). From each sample, 2 cm<sup>3</sup> were dissolved in water, bleached, wet-sieved and split into 90 μm, 120 μm and 180 μm fractions. Sedimentary charcoal particles were counted and categorized into: 1) poaceae (grass), 2) forbs (other herbaceous plants) and 3) wood (ligneous material) morphotypes following the methodology highlighted in Feurdean and Vasiliev (2019). The charcoal counts of each morphotype were transformed into percentages of the total charcoal counts.

## 4. Results

### 4.1. Temperatures

#### 4.1.1. SST estimates based on isoGDGTs

The amplitude of calculated SSTs in the Panagia record varies widely with a temperature variation of 17 °C (regardless of the choice of calibration; Fig. 3A; Supplementary Table 1). For the lower part of the record (0–360 m, 12.7–9.66 Ma) estimated SSTs average 20 °C and vary between 13 and 28 °C (TEX<sub>86</sub><sup>H</sup> calibration of Kim et al., 2010). For a short interval (330 to 360 m) temperatures raise remarkably attaining mean values of 27 °C. At 360 m the TEX<sub>86</sub><sup>H</sup> estimated SSTs drop rapidly and remain comparatively low, with an average value of 16 °C until the

top of the investigated section (630 m). When applying TEX<sub>86</sub><sup>L</sup> for <15 °C (i.e. polar and subpolar domains) for calculating SSTs the amplitude is slightly larger than when using TEX<sub>86</sub><sup>H</sup> (Fig. 3A; Supplementary Table 1). Notably, the overall trends observed when using TEX<sub>86</sub><sup>H</sup> calibration are mimicked by the TEX<sub>86</sub><sup>L</sup> (Fig. 3A). Considering the paleogeography of the section we will discuss the data using only the TEX<sub>86</sub><sup>H</sup> and refer to it as SST<sup>H</sup>.

#### 4.1.2. MAT' estimates based on brGDGTs

Measured MAT' values range from 14 to 20 °C with a mean of 17 °C (Fig. 3B; Supplementary Table 1). Between 120 and 350 m MAT' values increase by ~4 °C when compared to the Volhynian base of the section (0–10 m). From 10 to 120 m temperatures vary between 14 and 18 °C, with a mean value of ~16 °C. From 360 to 540 m MAT' varies between 14 and 19 °C with a mean of 17 °C. For the uppermost part (540–650 m) of the section mean MAT' values increase slightly to ~18 °C. There are root mean square errors on absolute MBT'/CBT-derived MAT' reconstructions on the order of 5 °C (Peterse et al., 2012), therefore we postulate that importance should be given to the relative MAT trends.

### 4.2. Compound specific stable isotope data

#### 4.2.1. Compound specific δ<sup>2</sup>H and δ<sup>13</sup>C data on alkenones

The first significant occurrence of alkenones in the record is at 344.3 m. Until this level alkenones are present in only three samples: at 14.50 m (TP 015), 192.2 m (TP 053) and at 290 m (TP 088). The alkenone concentration in these samples was, however, too low for isotope analysis.

**4.2.1.1. δ<sup>2</sup>H alkenone values.** δ<sup>2</sup>H values of C<sub>37</sub> alkenones (δ<sup>2</sup>H<sub>C37alkenones</sub>) range between –126 and –202‰ (Fig. 3C; Supplementary Table 2) and follow the same trend as δ<sup>2</sup>H values for C<sub>38</sub> alkenones (δ<sup>2</sup>H<sub>C38alkenones</sub>) showing a very good correlation (R<sup>2</sup> = 0.83, Supplementary Table 2) yet at slightly lower δ<sup>2</sup>H values (–125 to –191‰). The δ<sup>2</sup>H<sub>C37alkenones</sub> record starts with the highest value of –126‰ at 354 m and is followed by a drop to –169‰, increasing again to –145.4‰ at 408.9 m. After 416 m a pronounced negative excursion in δ<sup>2</sup>H<sub>C37alkenones</sub> occurs with values ranging from –176‰ to –202‰ and a mean of 186‰ (454–560 m). Between 560 and 600 m, δ<sup>2</sup>H<sub>C37alkenones</sub> and δ<sup>2</sup>H<sub>C38alkenones</sub> increase again, to values attaining a maximum of –129‰. After 600 m the δ<sup>2</sup>H<sub>C37alkenones</sub> decrease sharply from –149‰ to –188‰ and stay at low values until the end of the section, albeit with an accentuated variability (±26‰).

**4.2.1.2. δ<sup>13</sup>C alkenones.** δ<sup>13</sup>C values of C<sub>37</sub> alkenones (δ<sup>13</sup>C<sub>C37alkenones</sub>) vary between –20.5‰ and –26.1‰ (Fig. 3D; Supplementary Table 3) while δ<sup>13</sup>C values of C<sub>38</sub> alkenones (δ<sup>13</sup>C<sub>C38alkenones</sub>) fall between –20.2‰ and –26.5‰. Similar to the δ<sup>2</sup>H record, δ<sup>13</sup>C<sub>C38alkenones</sub> values follow the same trend as the δ<sup>13</sup>C<sub>C37alkenones</sub> showing a strong correlation (R<sup>2</sup> = 0.89, Supplementary Table 3). In the 350 m to 416 m interval δ<sup>13</sup>C<sub>C37alkenones</sub> and δ<sup>13</sup>C<sub>C38alkenones</sub> values decrease gradually from –20.5‰ to –23.5‰. Up section, δ<sup>13</sup>C<sub>C37alkenones</sub> values drop to –25.5‰ and remain low with an average of –24.9‰ (except sample TP183, at 454.95 m).

#### 4.2.2. Compound specific δ<sup>13</sup>C and δ<sup>2</sup>H values on *n*-alkanes

**4.2.2.1. δ<sup>13</sup>C values of long chain *n*-alkanes.** Long chain *n*-alkanes within the Panagia section show a clear odd over even predominance indicating a higher plant wax origin (Eglinton and Hamilton, 1967). δ<sup>13</sup>C values of C<sub>29</sub> *n*-alkanes (δ<sup>13</sup>C<sub>C29n-alkanes</sub>) range between –33.6‰ and –28.9‰ (Fig. 3E; Supplementary Table 3). Up to 300 m, δ<sup>13</sup>C<sub>C29n-alkanes</sub> values fluctuate between –33.2‰ and –30.1‰ attaining a mean of –31.5‰. After 300 m we observe a gradual increase in δ<sup>13</sup>C<sub>C29n-alkanes</sub> from –33.2 to –29.2‰ at 425.18 m, followed by a rapid and sharp drop to –32.7‰

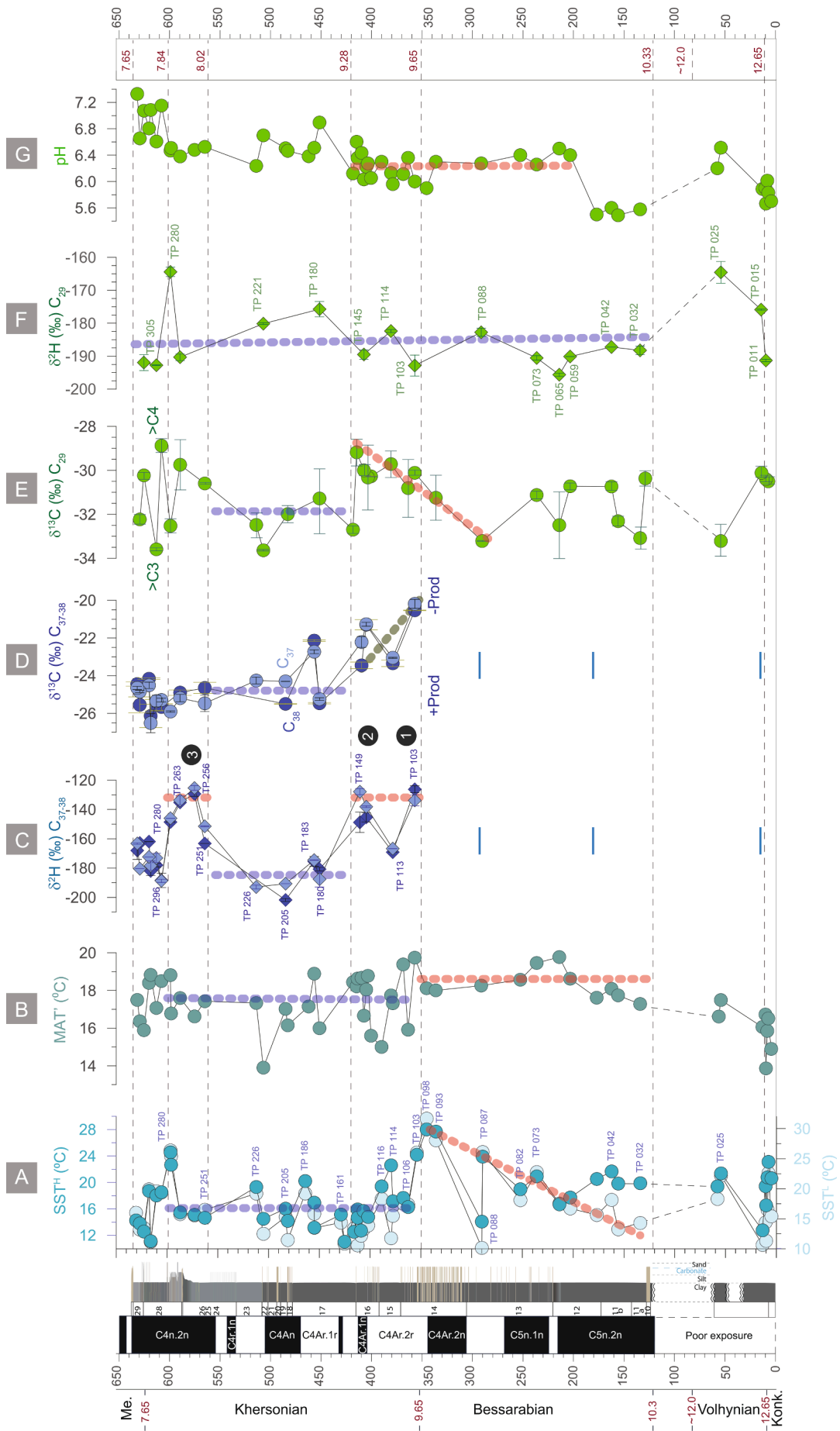


**Fig. 3.** Schematic lithologic and magnetostratigraphic logs together with summarized results from GDGTs, alkenones and *n*-alkanes. A) Sea surface temperature (SST<sup>H</sup>); B) Mean annual temperature (MAT); C)  $\delta^{2}\text{H}_{\text{C}_{37}\text{alkenones}}$  and  $\delta^{13}\text{C}_{\text{C}_{38}\text{alkenones}}$ ; D)  $\delta^{13}\text{C}_{\text{C}_{37}\text{alkenones}}$  and  $\delta^{13}\text{C}_{\text{C}_{38}\text{alkenones}}$ . No alkenones detected below 350 m except of traces in 3 samples (blue lines); E)  $\delta^{13}\text{C}_{\text{C}_{29n}\text{-alkanes}}$  and F)  $\delta^{2}\text{H}_{\text{C}_{29n}\text{-alkanes}}$ ; G) Paleo soil pH derived from GDGTs. The stratigraphic levels are in m. The main trends are marked on the figure with dashed lines. Additionally, the drying events are marked (black circles,  $\delta^{2}\text{H}_{\text{alkenones}}$  plot) and the names of the regional (sub)stages. Error bars are based on the standard deviation of a series of replicate analyses. Dashed colored lines indicate the main values trends. (For interpretation of the references to colour in this figure legend, the reader is referred to the web version of this article.)

at 428.70 m (Fig. 3E). Between 430 and 560 m  $\delta^{13}\text{C}_{\text{C}_{29n}\text{-alkanes}}$  values remain low and range between  $-30.6$  and  $-33.6\text{‰}$ . Towards the top of the section (560 m to 630 m)  $\delta^{13}\text{C}_{\text{C}_{29n}\text{-alkanes}}$  values are characterized by high variability. With a range of  $-28.9$  to  $-33.6\text{‰}$  they cover almost the entire spectrum of  $\delta^{13}\text{C}_{\text{C}_{29n}\text{-alkanes}}$  values recovered over the remainder of the section. In general,  $\delta^{13}\text{C}_{n\text{-alkanes}}$  values of  $\text{C}_{31}$  *n*-alkanes ( $\delta^{13}\text{C}_{\text{C}_{31n}\text{-alkanes}}$ ) parallel the  $\delta^{13}\text{C}_{\text{C}_{29n}\text{-alkanes}}$  record, yet at slightly lower absolute values.  $\delta^{13}\text{C}_{\text{C}_{29n}\text{-alkanes}}$  and  $\delta^{13}\text{C}_{\text{C}_{31n}\text{-alkanes}}$  values co-vary, showing a very good correlation ( $R^2 = 0.84$ , Supplementary Table 3).

**4.2.2.2.  $\delta^2\text{H}$  of long chain *n*-alkanes.**  $\delta^2\text{H}$  values of  $\text{C}_{29}$  *n*-alkanes ( $\delta^2\text{H}_{\text{C}_{29n}\text{-alkanes}}$ ) range between  $-164\text{‰}$  and  $-196\text{‰}$  (Fig. 3F; Supplementary Table 2) with an average value of  $-185\text{‰}$ . Between 0 and 120 m the  $\delta^2\text{H}_{\text{C}_{29n}\text{-alkanes}}$  values vary between  $-165\text{‰}$  and  $-191\text{‰}$  with a gradual increase from  $-191\text{‰}$  at 14.9 m to  $-165\text{‰}$  at 120 m. Between 120 m and 630 m  $\delta^2\text{H}_{\text{C}_{29n}\text{-alkanes}}$  values fall within a relatively narrow range ( $-176\text{‰}$  to  $-196\text{‰}$ ; except one positive excursion to  $-164\text{‰}$  at 596 m) attaining a mean  $\delta^2\text{H}_{\text{C}_{29n}\text{-alkanes}}$  value of  $185\text{‰}$ . The  $\delta^2\text{H}_{\text{C}_{29n}\text{-alkanes}}$  values are consistently slightly less negative than their  $\text{C}_{31}$  counterparts ( $\delta^2\text{H}_{\text{C}_{31n}\text{-alkanes}}$ ; Supplementary Table 2).  $\delta^2\text{H}_{\text{C}_{29n}\text{-alkanes}}$  and  $\delta^2\text{H}_{\text{C}_{31n}\text{-alkanes}}$  values co-vary, showing a strong correlation ( $R^2 = 0.84$ , Supplementary Table 2).  $\delta^2\text{H}$  values of  $\text{C}_{29}$  *n*-alkanes ( $\delta^2\text{H}_{\text{C}_{29}}$ ) range between  $-164\text{‰}$  and  $-196\text{‰}$  (Fig. 3F; Supplementary Table 2) with an average value of  $-185\text{‰}$ . Between 0 and 120 m the  $\delta^2\text{H}_{\text{C}_{29}}$  values vary between  $-165\text{‰}$  and  $-191\text{‰}$  with a gradual increase from  $-191\text{‰}$  at 14.9 m to  $-165\text{‰}$  at 120 m. Between 120 m and 630 m  $\delta^2\text{H}_{\text{C}_{29}}$  values fall within a relatively narrow range ( $-176\text{‰}$  to  $-196\text{‰}$ ; except one positive excursion to  $-164\text{‰}$  at 596 m) attaining a mean  $\delta^2\text{H}_{\text{C}_{29}}$  value of  $185\text{‰}$ . The  $\delta^2\text{H}_{\text{C}_{29}}$  values are consistently slightly less negative than their  $\text{C}_{31}$  counterparts ( $\delta^2\text{H}_{\text{C}_{31n}\text{-alkanes}}$ ; Supplementary Table 2).  $\delta^2\text{H}_{\text{C}_{29}}$  and  $\delta^2\text{H}_{\text{C}_{31}}$  values co-vary, showing a strong correlation ( $R^2 = 0.84$ , Supplementary Table 2).

#### 4.3. Soil pH

Paleo-soil pH values show an overall increasing trend over the course of the section, with pH values increasing from 5.7 (0–20 m) to ca. 7.3 (600–640 m) (Fig. 3G; Supplementary Table 1). In the lower part (0–120 m) of the section the pH values fluctuate between 5.6 and 6.5 followed by values typical for more acidic soils (5.5–5.6) at 120–180 m. After 180 m soil pH values increase sharply to 6.4 and maintain within a range of 5.9 to 6.4 until 420 m. Between 420 and 650 m soil pH values increase steadily up to a maximum value of 7.3 at 630.43 m.

#### 4.4. Charcoal

The samples show a well-preserved charred material with Poaceae as the most abundant morphotype in the record, followed by herbaceous and wood types (Fig. 4E; Supplementary Table 4). The percentage of Poaceae-derived material varies between 0 and 100%, with the highest abundance (80–100%) at 0–53 m, 200–250 m, 340–490 m and 544 m, and a maximum at 454 m (66 particles/cm<sup>3</sup> representing 85.7% of the total charcoal in the sample). Herbaceous charcoal morphotypes generally follow the trends of Poaceae. Their abundance varies between 0 and 100% (0–17 particles/cm<sup>3</sup>), with the maximum of charred material at 454 m. Wood morphotypes are less represented in the section and vary between 0 and 67% (0–12 particles/cm<sup>3</sup>), with the highest peak at 54 m, accounting for 37.8% of the total charcoal (Fig. 4E;

Supplementary Table 4). Results from charcoal morphology concentrations and sediment accumulation rates show no significant correlation.

### 5. Discussion: paleoenvironmental changes between 12.7 and 7.65 Ma

The absolute age constraints for the Panagia section are based on the magnetostratigraphic pattern comprising nine normal and eight reversed polarity intervals with additional seven short-term polarity fluctuations (Palcu et al., 2021) that were correlated to the geomagnetic polarity time scale (GPTS; Hilgen et al., 2012; Ogg, 2020). The transition between Konkian and Volhynian dated at 12.65 Ma (Palcu et al., 2017) is located at 2 m in the section. The interval between 2 and 120 m has poor exposure. The outcropping levels pin the 2 to 60 m interval to Volhynian, while the transition to Bessarabian, at  $\sim 12$  Ma, must be located in the exposure gap between 60 and 120 m. A straightforward correlation follows. The 120–250 m part of the section covers a long normal polarity interval that correlates to C5n.2n of the GPTS. Upward tuning pins the Bessarabian–Khersonian boundary (at 310 m) at 9.65 Ma. The long dominantly reversed interval between 360 and 480 m correlates to C4Ar and locates the Khersonian–Maeotian boundary in C4n.1r (625 m) at 7.65 Ma (Palcu et al., 2021). Based on these magnetostratigraphic constraints, the age of each sample was calculated by linear interpolation of the sample levels between the corresponding magnetic chron boundaries. Further, the geochemical proxy results were plotted based on the calculated ages (Fig. 5).

#### 5.1. Sea surface and continental temperature changes

Overall the Panagia SST<sup>H</sup> data reveal temperatures higher than the present-day values of 14 °C at the site. SST<sup>H</sup> values range from 14 to 28 °C for the interval between 10.3 and 9.68 Ma, a time interval representing most of the Bessarabian substage (Fig. 5A). After increasing temperatures lasting more than 0.5 Myr, a first rapid increase in SST<sup>H</sup> changes marks the end of the Bessarabian substage, at 9.7 Ma, when the SST<sup>H</sup> record reaches the highest values of 28 °C, followed by a consecutive warming with SST<sup>H</sup> of 24 °C (peaking at 9.57 Ma). This entire warm interval is preceded by an abrupt drop (from 24 to 14 °C) at 9.8 Ma (Fig. 5A). After 9.66 Ma the record shows low SST<sup>H</sup> fluctuations (around 16 °C) until 7.81 Ma. A third prominent SST<sup>H</sup> warming peak of  $\sim 9$  °C is observed in the upper(most) Khersonian (596.47 m) at 7.85 Ma, an interval corresponding to the so-called Great Khersonian Drying (Palcu et al., 2019, 2021). Between 7.85 Ma and 7.66 Ma SST<sup>H</sup> values range between 13.8 and 24.6 °C, with an upward cooling trend. This interval corresponds to the Maeotian transgression, a presumably humid phase (Popov et al., 2016; Palcu et al., 2019) that led to the reconnection with Dacian Basin at 7.65 Ma.

The brGDGT-based MAT reconstructions broadly follow the SST record (Fig. 3B) with MAT values expectedly higher than the present-day values of 11 °C at the site. For the largest part of the Bessarabian (10.3 and 9.79 Ma), a slight increase in temperature (17 to 19 °C) can be observed, while after the onset of the Khersonian, at 9.65 Ma, MAT varies around 17 °C. The only available record in Paratethys, partially overlapping in time with Panagia section, is the DSDP 42B 380 core from central Black Sea (Vasiliev et al., 2020). The interval from the DSDP tentatively correlated to 10 to 8 Ma (Vasiliev et al., 2020) shows values that are slightly lower (14 °C) than those recorded in Panagia (17 °C) specifically for the interval from 9.64 to 7.65 Ma. In the vicinity of the

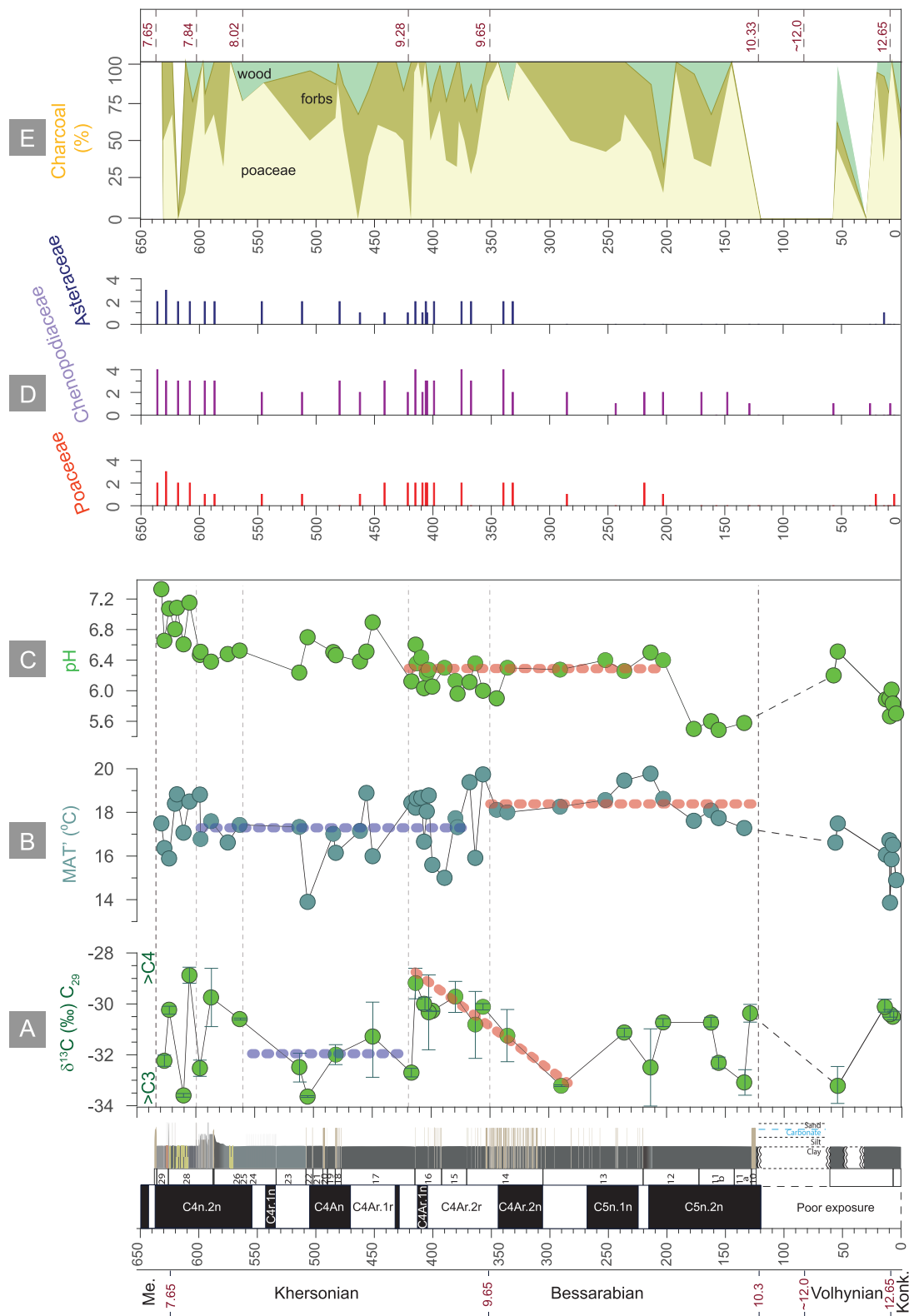


**Fig. 4.** Summarized continental signals. A)  $\delta^{13}C_{C29n}$ -alkanes; B) MAT; C) pH; D) Pollen (Razumkova, 2012) for taxa specific to open land/dry environments (Poaceae, Chenopodiaceae and Asteraceae). The numbers show the relative abundance, where 1 is for present, 2 for rare, 3 for common, and 4 indicates abundant; E) Fire regime reconstruction based on the preserved charcoal. The lithologic and magnetostratigraphic logs, as well as the names of regional substages are presented. Dashed colored lines indicate the main trends.

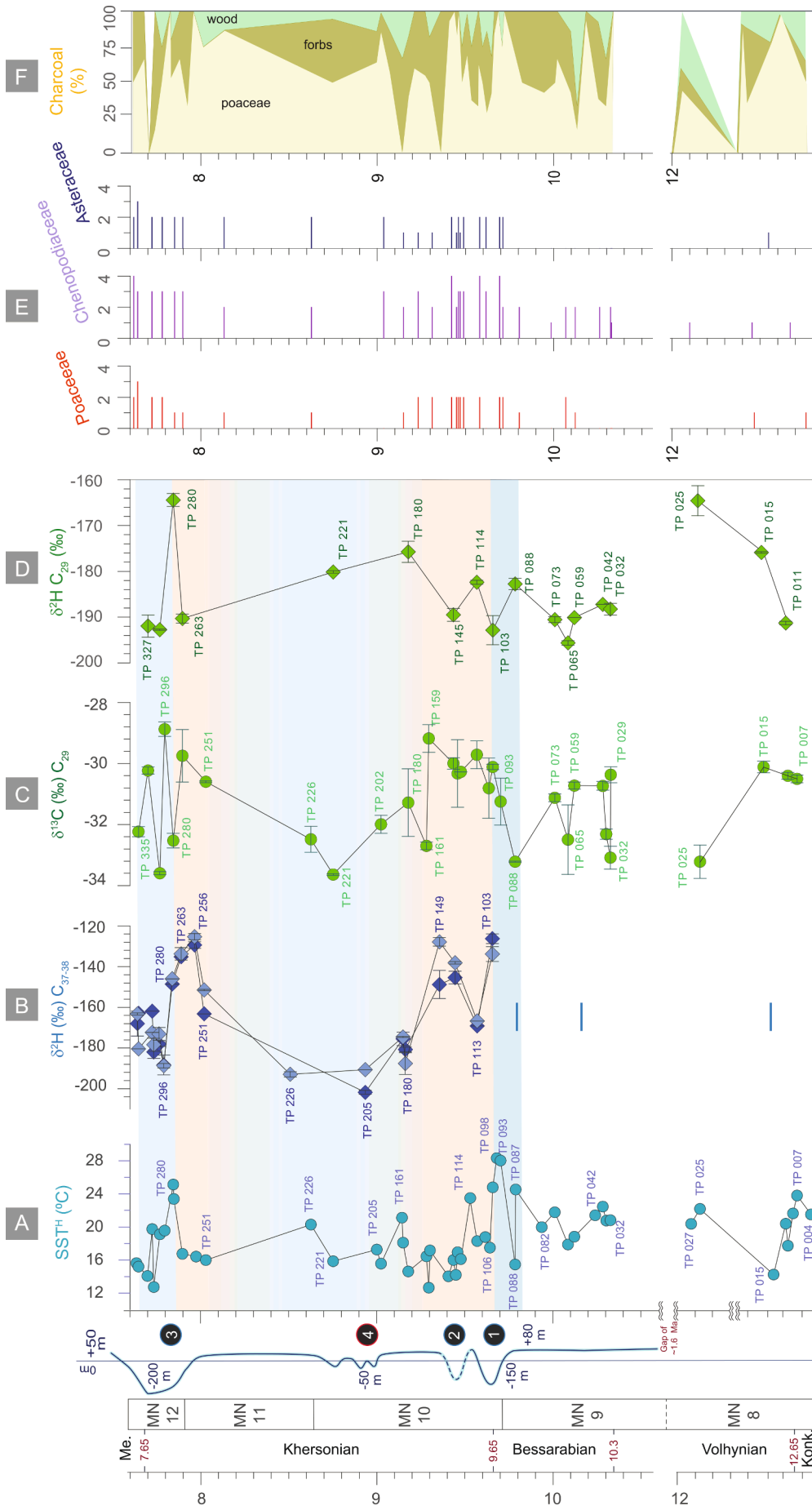


**Fig. 5.** Summarized organic geochemistry, pollen and charcoal data. A) SST<sup>H</sup> derived from GDGTs; B) δ<sup>2</sup>H<sub>C37alkenones</sub>; C) δ<sup>13</sup>C<sub>29n-alkanes</sub>; D) δ<sup>2</sup>H<sub>C29n-alkanes</sub>; E) Selected pollen (Razumkova, 2012) where numbers show the relative abundance, with 1 present, 2 rare, 3 common, and 4 abundant; F) Charcoal. Ages are in million years (Ma). The main environmental changes and their ages are indicated. With orange bars are depicted the main drying periods, while in blue are the wetter periods. The black circles with blue borders represent the observed dry phases (1–3), while red border marks a fourth event cf. [Palcu et al. \(2021\)](#). Blue lines on the δ<sup>2</sup>H<sub>C37alkenones</sub> column mark occasional levels with alkenone occurrence. Dashed lines represent the main trends. The section records a gap of ~1.6 Ma during the Volhynian stage. MN refers to Miocene mammal zones. (For interpretation of the references to colour in this figure legend, the reader is referred to the web version of this article.)

Black Sea, paleobotanical data using coexistence approach estimate similar MAT values of 13.3–17 °C for the Serravallian–Tortonian for sites in Bulgaria and the Ukrainian Carpathians, while lower values of 9–10 °C are depicted for the Ukrainian Plains sites (Ivanov et al., 2011; Syabryaj et al., 2007).

The rapid and large (~14 °C, 9.79–9.68 Ma) SST<sup>H</sup> temperature increase prior to the 9.68–9.66 Ma warm interval is remarkable and may have been triggered either by 1) a period of regional warming, 2) a connection to a neighboring warm (marine) basin through a major gateway (Fig. 6A–D), or 3) a period of prolonged drought and warming

of the Paratethys basin in concert with basin isolation (Fig. 6E–H).

1) The absence of large MAT fluctuations coeval to the large SST variation between 9.75 and 9.66 Ma suggests that the warming occurred only in the aquatic domain. Regional transient warming seems to be an unlikely candidate to explain the 14 °C warming of the Paratethys surface waters as age-equivalent brGDGT-based MAT reconstructions indicate that the 9.68–9.66 Ma interval represents the termination of a prolonged time interval (10.3 Ma to 9.66 Ma) of rather constant MAT prior to an overall MAT decrease in concert with SST<sup>H</sup> post 9.66 Ma (Fig. 3).

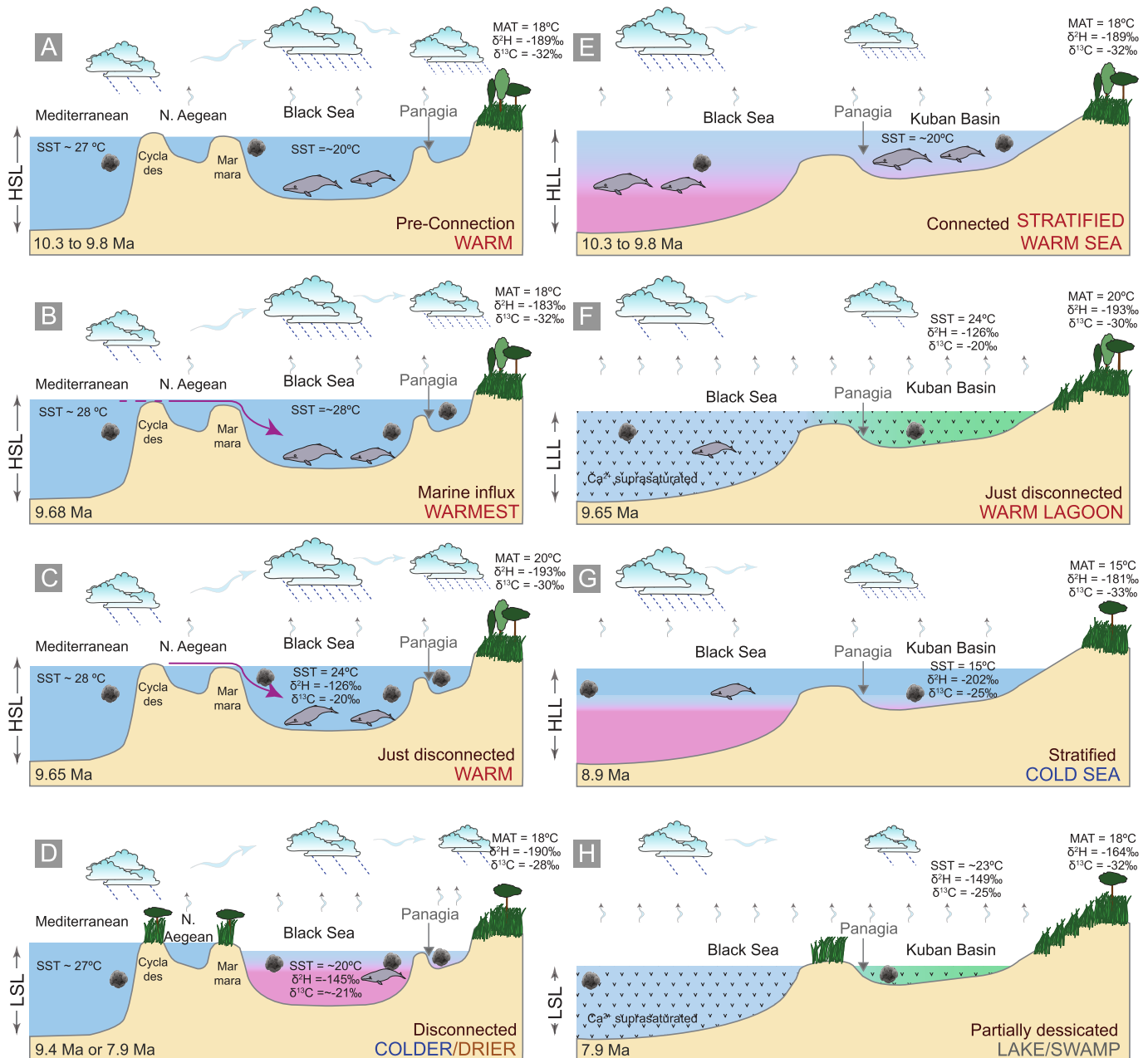


**Fig. 6.** Schematic scenarios at different times corresponding with events found in Panagia section. A–D scenarios based on a short connection with another basin at 9.68 Ma followed by complete isolation (Mediterranean SST values from Tzanova et al., 2015), while E–H scenarios assume isolation with no possible connection to another marine basin at 9.68 Ma. A) 10.3–9.8 Ma a warm East Paratethys disconnected from the global ocean; B) At 9.68 Ma, a short connection with a warmer water body is established (possibly the Mediterranean via proto-Aegean); C) At 9.65 Ma the connection is closed; D) At 9.4 and 7.9 Ma the basin becomes isolated again, but in a colder and dryer environment; E) Between 10.3 and 9.8 Ma the basin becomes stratified due to isolation; F) At ~9.65 Ma the basin experiences a strong regression that transforms marginal realms in poorly connected lagoons or marginal lakes, increase salinity and mineral content in the central basin with negative impacts on the biota; G) After the first crisis the basin experiences a partial recovery during colder and more humid periods; H) The regression trend culminates at ~7.9 Ma when the areas of Panagia become coastal-swamp environments. Please note that the proximity of the Panagia section to terrestrial sources changes greatly throughout the above-mentioned episodes. Abbreviations: HSL – High Sea Level; LSL – Low Sea Level, HLL – High Lake Level, LLL – Low Lake Level.



2) If the rapid SST<sup>H</sup> increase between 9.75 and 9.66 Ma was provoked by a connection to a basin supplying a substantial influx of warm waters in <100 kyr, the source must have been a large waterbody since it provoked such a SST change. This interval is marked by the occurrence of *Coccolithus pelagicus* (Popov et al., 2016), an alkenone producer thriving in open marine environments. While alkenones are usually absent from analyzed samples prior to 9.66 Ma, they are continuously reported after this interval. The presence of alkenones could be explained by a model where alkenone producers were introduced by the warm waters derived from a neighboring (marine) basin. Additionally, the coeval appearance of *Actinopteryx annulatus*, a tropical marine diatom species (Popov et al., 2016), supports the interpretation of an influx of warm marine waters into the Eastern Paratethys. The exact location of the associated marine gateway remains speculative though. During the late Miocene, the Paratethys domain was an active tectonic area with changing connectivity. Previously active Miocene connections through the Transtethyan corridor (in Slovenia; Sant et al., 2017) and Barlad (Romania, Palcu et al., 2017) closed during Bessarabian (~12–9.65 Ma). A gateway between the Black Sea and the Dardanelles existing at ~9 Ma (Krijgsman et al., 2020) may have been too small to generate such important changes in Paratethys SSTs.

3) An alternative explanation for the 9.68–9.66 Ma SST<sup>H</sup> warm interval could be a period of prolonged drought and isolation of the Paratethys, leading to a smaller residual water volume in the basin, easier to warm up. Paratethys basin level fluctuated by more than 200 m between the wet and the dry intervals (Palcu et al., 2021). During Paratethys low stands, the area of Panagia switched from deep water to lagoon, coastal swamp and ultimately terrestrial environments (Popov et al., 2006). The high SST<sup>H</sup> values could be explained by the installation of shallow water conditions (e.g. lagoonal, coastal). The short-lived warming of the Paratethys basin in the Panagia region however, would not explain the sudden occurrence of alkenone producers and their sustained (post-9.66 Ma) presence in a rather evaporative basin. Continuous drying could have led to increased salinity in the Black Sea/Kuban basin, to values close to normal marine. Possibly, some alkenone producers may have survived previously (as suggested by the TP 015 (12.49 Ma), TP 053 (10.17 Ma) and TP 088 (9.79 Ma) containing traces of alkenones) in ecological niches (e.g. Georgian part of the Black Sea), then expanded in the Paratethys when conditions became suitable.

## 5.2. Hydrological changes: periods of prolonged and intensive drought

Three periods characterized by extremely high  $\delta^2\text{H}_{\text{C}_{37}\text{alkenones}}$  values (corresponding to dry periods) occur within the Panagia record (Figs. 3C, 5B; Supplementary Table 2): the first one ( $\delta^2\text{H}_{\text{C}_{37}\text{alkenones}}$  –126‰ at 354 m) occurs at the end of the Bessarabian (9.66 Ma), while the second interval (–149‰ at 415.85 m) follows at 9.41 Ma, shortly after the beginning of Khersonian. The third interval, where  $\delta^2\text{H}_{\text{C}_{37}\text{alkenones}}$  attains values as high as –129.4‰, occurs at the end of the Khersonian (8.03–7.79 Ma).

Similarly high  $\delta^2\text{H}_{\text{C}_{37}}$  values have been reported only from the Mediterranean basin during the Messinian Salinity Crisis (5.97–5.33 Ma), an event characterized by basin-wide massive evaporation ( $\delta^2\text{H}_{\text{C}_{37}\text{alkenones}}$  of –140 to –120‰; Vasiliev et al., 2017). In the Black Sea region comparable  $\delta^2\text{H}_{\text{C}_{37}\text{alkenones}}$  values (–145‰) were reported in two other sites: Zheleznyi Rog (~10 km east of Panagia section; Vasiliev et al., 2013, 2020) and the deep Black Sea at DSDP 42B site 380 hole (Vasiliev et al., 2015). These sites both document a late Sarmatian (s.l.) interval with elevated  $\delta^2\text{H}_{\text{C}_{37}\text{alkenones}}$ . Given the uncertainties on the Zheleznyi Rog and DSDP 42B 380 age models, we tentatively correlate these intervals with the late Khersonian of the Panagia section (562 to 605 m), between 8.02 and 7.79 Ma. Consequently, we interpret the high  $\delta^2\text{H}_{\text{C}_{37}\text{alkenones}}$  values as an expression of enhanced evaporation affecting the Paratethys basin. Considering that present-day marine  $\delta^2\text{H}_{\text{C}_{37}\text{alkenones}}$  values are rarely higher than –180‰ (e.g. in the warm Sargasso Sea at 31° N; Englebrecht and Sachs, 2005; Weiss et al., 2019)

evaporative Paratethys water loss must have outpaced rainout and runoff from the basin catchment.

In between the main intervals with high  $\delta^2\text{H}_{\text{C}_{37}\text{alkenones}}$  (9.66–9.41 Ma and 8.02–7.79 Ma), MAT and SST<sup>H</sup> data indicate a colder climate and  $\delta^2\text{H}_{\text{C}_{37}}$  values attain –176 to –202‰. These are found in the present day open marine settings, while the  $\delta^2\text{H}_{\text{C}_{37}\text{alkenones}}$  of more restricted Black Sea basin reaches –230‰ (van der Meer et al., 2008). Based on the sedimentological record within the 8.57–9 Ma time period, an additional drying event, of smaller intensity, has been described in Panagia (Palcu et al., 2021). We were unable to identify this event in the organic geochemistry data possibly due to the lower sampling resolution. All warming events observed in the Panagia section are accompanied by carbonate deposition (Palcu et al., 2021), suggesting coeval changes in the chemistry and circulation of the basin.

The  $\delta^{13}\text{C}_{\text{C}_{37}}$  values from Panagia (–26.5‰ to –20.5‰) are close to global upper Miocene values (–25‰ to –21‰) (e.g. Pagani et al., 1999), yet somewhat different to those measured in the recent Black Sea (–26‰ to –29‰) (e.g. Freeman and Wakeham, 1992). Important is the 3‰ decrease in  $\delta^{13}\text{C}_{\text{C}_{37}\text{alkenones}}$  (Fig. 3D, Supplementary Table 3) between 9.66 and 9.28 Ma, that parallels an increase in  $\delta^2\text{H}_{\text{C}_{37}}$  up to –126‰, a value typical for evaporative conditions. After 9.28 Ma, until the end of the record, the  $\delta^{13}\text{C}_{\text{C}_{37}\text{alkenones}}$  values are stable around –25‰, although between 8.03 and 7.79 Ma the  $\delta^2\text{H}_{\text{C}_{37}}$  registers another marked increase up to –129.4‰. While the  $\delta^2\text{H}_{\text{C}_{37}\text{alkenones}}$  depends heavily on the hydrological conditions of a basin (e.g. evaporation vs. precipitation), the  $\delta^{13}\text{C}_{\text{C}_{37}\text{alkenones}}$  depends on the magnitude of the carbon isotopic fractionation in the sedimentary record. The latter is a function of various factors, including: 1) the concentration of aqueous CO<sub>2</sub>, 2) algal growth rates (Bidigare et al., 1997) and 3) the ratio of cellular carbon content to cell surface area (Popp et al., 1998) during late-stage exponential and stationary growth (Benthien et al., 2007). We can explain the 3‰ decrease between 9.66 and 9.28 Ma in the  $\delta^{13}\text{C}_{\text{C}_{37}\text{alkenones}}$  as a consequence of (a combination) of the three factors mentioned above, being enhanced by increasing evaporative conditions (i.e. high  $\delta^2\text{H}_{\text{C}_{37}\text{alkenones}}$ ). However, we speculate that the algal growth rate had a major role in determining the carbon isotopic fractionation. No significant changes in the concentration of aqueous CO<sub>2</sub> are known for the time interval to explain alone the 3‰ decrease, although paleo-pCO<sub>2</sub> reconstructions based on  $\delta^{13}\text{C}_{\text{C}_{37}\text{alkenones}}$  show an 80 ppm increase at ~9.5 Ma (Pagani et al., 1999), stabilizing afterwards at the pre-industrial levels by 9 Ma. The limited number of preserved coccoliths reported in Panagia (Popov et al., 2016) does not allow a reliable assessment of changes in the cell size. The rather constant  $\delta^{13}\text{C}_{\text{C}_{37}\text{alkenones}}$  between 8.03 and 7.79 Ma remains difficult to explain without identification of the alkenone producers.

## 5.3. Vegetation changes: expansion of grasslands

The  $\delta^{13}\text{C}$  values of plant waxes primarily reflect different vegetation types. Leaf wax long chain *n*-alkanes from C<sub>3</sub> plants have a mean  $\delta^{13}\text{C}$  value of –33.0‰, whereas those from C<sub>4</sub> plants (e.g. grasses, savannah, salt marsh and desert plants) are as high as –21.7‰ (e.g. Castañeda and Schouten, 2011; Feakins et al., 2020).

In the Panagia section, marked trends in  $\delta^{13}\text{C}_{\text{C}_{29}}$  reaching values up to –29‰ are observed between 9.66 and 9.28 Ma and 8.02–7.77 Ma. The high  $\delta^{13}\text{C}_{\text{C}_{29n}\text{-alkanes}}$  values between 9.66 and 9.28 Ma coincide with the interval of very high  $\delta^2\text{H}_{\text{C}_{37}\text{alkenones}}$  values suggesting that (regionally) dry conditions supported the spread of C<sub>4</sub> vegetation in the area surrounding the basin. It is also remarkable that the +2‰ shift in  $\delta^{13}\text{C}_{\text{C}_{29n}\text{-alkanes}}$  (i.e. terrestrial environment) (Fig. 3E, 5C) is opposite to the –3‰ shift in the alkenone  $\delta^{13}\text{C}_{\text{C}_{37}\text{alkenones}}$  (i.e. aquatic environment) data (Fig. 3D, Supplementary Table 3). The second interval with high  $\delta^{13}\text{C}_{\text{C}_{29n}\text{-alkanes}}$  values (8.02–7.77 Ma) also exhibits high variability in  $\delta^{13}\text{C}_{\text{C}_{29}}$  values that oscillate between –28.9‰ and –33.6‰. We interpret these fast changes as a consequence of repeated vegetation changes in the area surrounding the basin, from more C<sub>3</sub> plants ( $\delta^{13}\text{C}_{\text{C}_{29n}\text{-alkanes}}$

= -33.6‰) to an important contribution of C<sub>4</sub> plants ( $\delta^{13}\text{C}_{\text{C}_{29\text{n-alkanes}}} = -28.9\%$ ). Phytolith data indicate that C<sub>3</sub> grass-dominated savanna-mosaic vegetation had become widespread in Turkey and surrounding areas by the late Miocene (~9 Ma), while C<sub>4</sub> grasses were of little ecological importance in western Eurasia until at least the latest Miocene (~7 Ma) (e.g. Strömberg et al., 2007; Ivanov et al., 2002). To date, the oldest ecosystem dominated by C<sub>4</sub> grasses in Western Eurasia has been documented for the Pikermi Formation between 7.35 and 7.14 Ma (Böhme et al., 2017).

The Panagia pollen record (Razumkova, 2012) suggests an important change in the dominant vegetation through the increased abundance of Chenopodiaceae, Asteraceae and Poaceae pollen and of herbaceous charcoal morphologies during the Khersonian, especially during the three main drying events (Figs. 4D, 5E). Our charcoal record further indicates an increase in biomass burning and herbaceous morphotypes, supporting a dryer, more flammable ecosystem (Fig. 5F). Chenopodiaceae abundance also suggests a dry-saline environment (El-Moslimany, 1990) while the Asteraceae family (*Artemisia* in particular) is a newcomer that expands westwards from China (Wang, 2004). The occurrence and increased abundance of Asteraceae also hints at the expansion of a wider open landscape, favoured by a drying Paratethys. Interestingly, the increased dominance of herbaceous charcoal morphologies between 9.66 and 9.28 Ma (Fig. 5F; Supplementary Table 4) is coeval with the high  $\delta^2\text{H}_{\text{alkenones}}$  (i.e. excess evaporation), high  $\delta^{13}\text{C}_{\text{n-alkanes}}$  (i.e. more C<sub>4</sub> suggesting drier conditions), increasing paleo-soil pH (i.e. drier conditions) (Fig. 3G). The other time interval with similar data is during late Khersonian, between 8.02 and 7.79 Ma, when increased dominance of herbaceous charcoal morphologies is coeval with higher  $\delta^2\text{H}_{\text{alkenones}}$ , high  $\delta^{13}\text{C}_{\text{n-alkanes}}$ , and, in this case, increased paleo-soil pH (up to the highest values, averaging ~7), typical for drier conditions and open vegetation. The coeval 2‰ observed increasing trend in  $\delta^{13}\text{C}_{\text{C}_{29\text{n-alkanes}}}$ , opposing the decreasing  $\delta^{13}\text{C}_{\text{C}_{37\text{alkenones}}}$  by 3‰ is striking. The increase in  $\delta^{13}\text{C}_{\text{n-alkanes}}$  between 9.66 and 9.28 Ma (Figs. 4E; 5C) supports an increase of C<sub>4</sub> plant contribution as the global expansion of C<sub>4</sub> grasslands in the late Miocene has been attributed to a large-scale decrease in atmospheric CO<sub>2</sub> (Cerling et al., 1997). On the other hand, the 3‰ decrease in  $\delta^{13}\text{C}_{\text{alkenones}}$  in Panagia could be explained by a change in haptophytes physiology over time as the depositional environment changed.

Knowledge about vegetation changes has implications for the interpretation of the *n*-alkane  $\delta^2\text{H}$  data because the discrimination against deuterium (<sup>2</sup>H) during photosynthesis is greater in C<sub>3</sub> plants than in C<sub>4</sub> plants (Polissar and Freeman, 2010; Feakins and Sessions, 2010). Despite these physiology-induced limitations  $\delta^2\text{H}_{\text{n-alkanes}}$  values have been successfully used in reconstructions of  $\delta^2\text{H}$  of paleo precipitation (e.g. Sachse et al., 2004; Pagani et al., 2006; Niedermeyer et al., 2016).

Except for two samples (at 12.13 Ma and at 7.85 Ma) where  $\delta^2\text{H}_{\text{C}_{29\text{n-alkanes}}}$  values increase to ~ -164‰,  $\delta^2\text{H}_{\text{C}_{29\text{n-alkanes}}}$  values in the Panagia section average -185‰ with rather low ( $\pm 10\%$ ) variability. This low variability in  $\delta^2\text{H}_{\text{C}_{29\text{n-alkanes}}}$  suggests that the hydrogen isotopic composition of precipitation stayed rather constant within the basin catchment during the late Miocene. Particularly important in this context is sample TP 280 at 7.85 Ma (Fig. 5D). At this level highest  $\delta^2\text{H}_{\text{C}_{29\text{n-alkanes}}}$  values (ca. -164‰) coincide with high  $\delta^2\text{H}_{\text{C}_{37\text{alkenones}}}$  values of ca. -130‰, high SST<sup>H</sup> of 26 °C, high MAT of 19 °C and high  $\delta^{13}\text{C}_{\text{C}_{29\text{n-alkanes}}}$  values of -29‰. Collectively, these data indicate that exceptionally dry conditions coincided with an exceptionally warm period at 7.85 Ma.

Assuming rather constant rainfall  $\delta^2\text{H}$  values, the positive excursions in  $\delta^2\text{H}_{\text{C}_{37\text{alkenones}}}$  values at 9.66, 9.45–9.41 and 7.85–7.87 Ma support the idea that these elevated  $\delta^2\text{H}_{\text{C}_{37\text{alkenones}}}$  do not reflect increasing temperature within the basin water column, but are rather a consequence of episodic basin restriction with enhanced evaporation as a consequence of changes in basin hydrology or connectivity to adjacent basins. Such a scenario is supported by the observation that the overall stable  $\delta^2\text{H}_{\text{C}_{29\text{n-alkanes}}}$  values (for exceptions see above) do not mimic the

MAT and SST<sup>H</sup> temperature records (Figs. 4; 5), indicating that temperature change is not the driver for the drying phases between 9.66 and 9.41 Ma. Despite the warm SSTs and MATs, the most probable mechanism for basin-wide droughts at the onset of the Khersonian (9.65 Ma) is a change in connectivity resulting in basin isolation and regression.

In contrast, rather low SST<sup>H</sup> and low MAT<sup>H</sup> (16–18 °C) combined with increased evaporation (high  $\delta^2\text{H}_{\text{C}_{37\text{alkenones}}}$ ) and low  $\delta^2\text{H}_{\text{C}_{29\text{n-alkanes}}}$  values collectively indicate that the 7.93 Ma Great Khersonian Drying was associated with rather cool conditions, similarly to the increased negative water budget observed for the Mediterranean basin during glacial peaks centered around 5.8 and 5.6 Ma (Vasiliev et al., 2017).

#### 5.4. Timing of events in regional and global context

The time-intervals with dryer conditions recorded in Panagia (9.66–9.28 and 8.02–7.84 Ma) coincide with periods of mammal turnover and dispersal in Eurasia suggesting that major environmental changes occurred also in circum-Paratethys region, when periods of prolonged droughts generated biotic crises and animal displacements across the Eurasian continent.

Periods of drought observed in the Panagia record at 9.68–9.66 Ma closely coincide with the MN 9–MN 10 transition, at 9.7 Ma, known as the onset of the Vallesian Crisis (e.g. Fortelius et al., 2014), whose amplitude has been subsequently questioned. Casanovas-Vilar et al. (2014) propose that sampling and preservation bias led to an overrating of extinction rates for the Vallesian Crisis. However, important in the context is the first occurrence of murids in Europe, dispersed from southern Asia, a time-transgressive event connected to the opening of landscapes reaching Eastern Europe between 9.7 and 9.6 Ma (Van Dam, 1997; Wessels, 2009). The drought in Panagia at 9.68–9.66 Ma also corresponds to a diminishing hydrologic cycle observed between 9.7 and 9.5 Ma, when an Atlantic driving mechanism was proposed by Böhme et al. (2008) to explain the Europe transition from a washhouse to a dryer climate.

At Panagia,  $\delta^{13}\text{C}_{\text{C}_{29\text{n-alkanes}}}$  values indicate an increased contribution of C<sub>4</sub> plants adapted to drier conditions at 9.66 Ma. Similarly high  $\delta^{13}\text{C}_{\text{C}_{29\text{n-alkanes}}}$  values continue until 9.4 Ma, when in Western Europe increased seasonality accelerated the demise of the evergreen subtropical woodlands (Mosbrugger et al., 2005; Fortelius et al., 2014). The end of the Bessarabian (9.65 Ma) also corresponds to the maximum in dust mass accumulation rates typical of dry deposition announcing the onset of transient Arabian hyperaridity in the proximity of the Paratethys domain (Böhme et al., 2021). The other marked increased contribution of C<sub>4</sub> plants and excessive drought observed in Panagia between 8.02 and 7.84 Ma appears to be correlated to a second period of Arabian hyperaridity centred at 7.78 Ma (Böhme et al., 2021). Using a 3D paleogeographic model Palcu et al. (2021) calculated a ~ 70% loss of Paratethys surface and a ~ 33% volume reduction during regressions associated to the 9.66–9.28 and 8.02–7.84 Ma dry phases.

In the aquatic domain, the end of the Bessarabian (9.65 Ma) stands out as the moment when a large number of the endemic paratethyan cetaceans (dominated by baleen whales) become extinct, while the Cetotheriidae family dominated the Khersonian (Gol'din and Startsev, 2017). The Volhynian and Bessarabian whales (Gol'din and Startsev, 2017) partial extinction at the end of the Bessarabian coincides with an event observed in this contribution at ~9.7 Ma, the so-called bed 14 in Popov et al. (2016). Bed 14 in Panagia section is a peculiar layer containing remains of large baleen whales, small bones and wood fragments (Popov et al., 2016) and coincides with the marked shift in the SST<sup>H</sup> between at 9.68 and 9.66 Ma. The Bessarabian–Khersonian transition is also marked by a bivalve turnover in the Eastern Paratethys (Kojumdjieva and Popov, 1988), when assemblages containing *Plicatiforma fittoni* and small-sized *Cardium* bivalves are replaced by *Maetra* genus.

When compared to existing age-equivalent records from the marine Mediterranean (Tzanova et al., 2015), the northern Atlantic and the

Indian Ocean (Herbert et al., 2016), the Panagia record shows distinct similarities yet also important differences: 1) Paratethys SST<sup>H</sup> values are ~7 °C lower when compared to the Mediterranean Monte dei Corvi section (Italy, Tzanova et al., 2015, Supplementary fig. 3B), however, the temporal resolution of our record does not allow discriminating the short temperature drops depicted in the Monte dei Corvi SST record; 2) During the upper Khersonian and transition into Maeotian (around 7.7 Ma) we observe a similar cooling trend to the North Atlantic ODP 907 record (Supplementary fig. 3C); however with significantly warmer (~7 °C) Paratethys waters; 3) For the Bessarabian the overall trend is similar to the Indian Ocean ODP 722 record (Supplementary Fig. 3E) with water temperature only 3 °C higher in the Paratethys.

Collectively these observations support a model in which the Eastern Paratethys evolved as a largely (en)closed system, recording paleo-environmental signals that are governed by interbasinal connectivity (or lack of it) and regional climate change in the basin catchment. Acting as an important source of humidity for Western and Central Asia, the size and areal extent of the Paratethys water body, however, is likely to have had a major impact on hydroclimate patterns in the Eurasian interior (Ramstein et al., 1997). The cumulative fluctuations in both hydrology and surface temperature of Paratethys might have increased the aridity and additionally enhanced seasonality, with different partition of moisture over the year. Our combined data suggests a decoupling from the global system (Böhme et al., 2021), dominated by a local regional climate induced by tectonics and Paratethys volume and, more importantly, areal extent reduction.

## 6. Conclusions

The integrated temperature,  $\delta^2\text{H}$  and  $\delta^{13}\text{C}$  isotope compositions of *n*-alkanes and alkenones combined with charcoal data reveal distinctive environmental conditions during the late Miocene in the Eastern Paratethys of Central Eurasia from the well-dated Panagia section (Taman Peninsula, Russia). Based on the multiproxy approach, we observe a series of important environmental events:

- 1) Between 9.68 and 9.66 Ma a short event generated much warmer and most probably more saline waters in the Eastern Paratethys. This event caused alkenone producers to thrive and marks the end of the Bessarabian stage. The warming can be explained either by i) an alleged marine water influx introducing the alkenone producers into the basin (i.e. a connection to an adjacent water body, possibly Mediterranean via proto-Aegean), although the exact location remains speculative, or ii) a warming of the basin associated with salinity increase as consequence of isolation and water level drop (i.e. a switch from open sea to lagoon conditions).
- 2) Three major drying events are observed in the Panagia record: at 9.65 Ma, 9.4 Ma and 7.9 Ma. The three events are well expressed in high  $\delta^2\text{H}_{\text{alkenones}}$ , indicating increased evaporation.
- 3) At 9.6 Ma a change towards increased contribution of  $\text{C}_4$  plants occurs, indicating a gradual transition from forests towards open land vegetation. This interval is marked by an intensified fire activity in the area, as the charcoal concentration increases.
- 4) The onset of open type vegetation and the appearance of the Asteraceae plant family are likely to be the result of continentalisation and, possibly, increased seasonality.
- 5) Panagia section temperature trends do not follow those of the larger water bodies around Eurasia (Mediterranean, North Atlantic and Indian oceans), suggesting that the Eastern Paratethys evolved as a fragmented, closed and restricted basin(s), being subject to its own environmental conditions.

## Declaration of Competing Interest

The authors declare that they have no known competing financial interests or personal relationships that could have appeared to influence

the work reported in this paper.

## Acknowledgements

This work was financially supported by Netherlands Organization for Scientific Research (NWO) [grant 865.10.011] of W.K., by German Science Foundation (DFG) [grant VA 1221/2-1] of I.V. and Senckenberg Gesellschaft für Naturforschung. D.P. acknowledges the Fundação de Amparo à Pesquisa do Estado de São Paulo (FAPESP) for financial support [grant 2018/20733-6]. I.V. and W.K. thank the sampling team (A. Iosifidi, V. Popov, S. Popov and M. Stoica) during 2005–2006 campaigns. G.B. and I.V. thank Ulrich Treffert for support in the SBiK-F organic geochemistry laboratory. Special thanks from G.B. to the Department of Marine Microbiology and Biogeochemistry (NIOZ). We also thank the two anonymous reviewers for their constructive suggestions that improved the original manuscript.

## Appendix A. Supplementary data

Supplementary data to this article can be found online at <https://doi.org/10.1016/j.gloplacha.2021.103644>.

## References

- Benthien, A., Zondervan, I., Engel, A., Hefter, J., Terbrüggen, A., Riebesell, U., 2007. Carbon isotopic fractionation during a mesocosm bloom experiment dominated by *Emiliania huxleyi*: Effects of CO<sub>2</sub> concentration and primary production. *Geochim. Cosmochim. Acta* 71 (6), 1528–1541.
- Bigdare, R.R., Fluegge, A., Freeman, K.H., Hanson, K.L., Hayes, J.M., Hollander, D., Jasper, J.P., King, L.L., Laws, E.A., Milder, J., Millero, F.J., Pancost, R., Popp, B.N., Steinberg, P.A., Wakeham, S.G., 1997. Consistent fractionation of <sup>13</sup>C in nature and in the laboratory: growth-rate effects in some haptophyte algae. *Glob. Biogeochem. Cycles* 13 (1), 251–252.
- Böhme, M., Ilg, A., Winkhofer, M., 2008. Late Miocene ‘washhouse’ climate in Europe. *Earth Planet. Sci. Lett.* 275, 393–401.
- Böhme, M., Spassov, N., Ebner, M., Geraads, D., Hristova, L., Kirscher, U., Kötter, S., Linnemann, U., Prieto, J., Roussiakis, S., Theodorou, G., Uhlir, G., Winkhofer, M., 2017. Messinian age and savannah environment of the possible hominin *Graecopithecus* from Europe. *PLoS One* 12 (5), e0177347. <https://doi.org/10.1371/journal.pone.0177347>.
- Böhme, M., Spassov, N., Majidifard, M.R., Gärtner, A., Kirscher, M., Dietzel, C.U., Uhlir, G., El Atfy, H., Begun, D.R., Winkhofer, M., 2021. Neogene hyperaridity in Arabia drove the directions of mammalian dispersal between Africa and Eurasia. *Nature Commun. Earth Environ.* 2, 85. <https://doi.org/10.1038/s43247-021-00158-y>.
- Casanovas-Vilar, I., van den Hoek Ostende, L.W., Furio, M., Madern, P.A., 2014. The range and extent of the Vallesian Crisis (late Miocene): new prospects based on the micromammal record from the Vallès-Penedès basin (Catalonia, Spain). *J. Iber. Geol.* 40 (1), 29–48. <https://doi.org/10.5209/rev/JIGE.2014.v40.n1.44086>.
- Castañeda, I.S., Schouten, S., 2011. A review of molecular organic proxies for examining modern and ancient lacustrine environments. *Quat. Sci. Rev.* 30, 2851–2891.
- Cerling, T.E., Harris, J.M., MacFadden, B.J., Leakey, M.G., Quade, J., Eisenmann, V., Ehleringer, J.R., 1997. Global vegetation change through the Miocene/Pliocene Boundary. *Nature* 389, 153–158.
- De Jonge, C., Hopmans, E.C., Zell, C.I., Kim, J.-H., Schouten, S., Sinnighe Damsté, J.S., 2014. Occurrence and abundance of 6-methyl branched glycerol dialkyl glycerol tetraethers in soils: Implications for palaeoclimate reconstruction. *Geochim. Cosmochim. Acta* 141, 97–112.
- Eglinton, G., Hamilton, R.J., 1967. Leaf Epicuticular Waxes. *Science* 156, 1322–1335.
- El-Moslimany, A.P., 1990. Ecological significance of common nonaraboreal pollen: examples from drylands of the Middle East. *Rev. Paleobot. Palynol.* 64, 343–350.
- Englebrecht, A.C., Sachs, J.P., 2005. Determination of sediment provenance at drift sites using hydrogen isotopes and unsaturation ratios in alkenones. *Geochim. Cosmochim. Acta* 69 (17), 4253–4265.
- Feakins, S.J., Sessions, A.L., 2010. Controls on the D/H ratios of plant leaf waxes in an arid ecosystem. *Geochim. Cosmochim. Acta* 74, 2128–2141.
- Feakins, S.J., Liddy, H.M., Tauxe, L., Galy, V., Feng, X., Tierney, J.E., Miao, Y., Warny, S., 2020. Miocene C<sub>4</sub> grassland expansion as recorded by the Indus Fan. *Paleoceanogr. Paleoclimatol.* 35 <https://doi.org/10.1029/2020PA003856> e2020PA003856.
- Feurdean, A., Vasiliev, I., 2019. The contribution of fire to the late Miocene spread of grasslands in eastern Eurasia (Black Sea region). *Sci. Rep.* 9, 6950.
- Fortelius, M., Eronen, J.T., Kaya, F., Tang, H., Raia, P., Puolamäki, K., 2014. Evolution of Neogene mammals in Eurasia: environmental forcing and biotic interactions. *Annu. Rev. Earth Planet. Sci.* 42, 579–604.
- Freeman, K.H., Wakeham, S.G., 1992. Variations in the distributions and isotopic compositions of alkenones in Black Sea particles and sediments. *Org. Geochem.* 19 (1–3), 27–285.

- Gol'din, P., Startsev, D., 2017. A systematic review of cetother baleen whales (CetaceaCetotheriidae) from the late Miocene of Crimea and Caucasus, with a new genus. *Papers Palaeontol.* 3 (1), 49–68.
- Herbert, T.D., Lawrence, K.T., Tzanova, A., Cleaveland-Peterson, L., Gabalero-Gill, R., Kelly, K.S., 2016. Late Miocene global cooling and the rise of modern ecosystems. *Nat. Geosci.* 9, 843–847.
- Hilgen, F.J., Lourens, L.J., Van Dam, J.A., Beu, A.G., Boyes, A.F., Cooper, R.A., Krijgsman, W., Ogg, J.G., Piller, W.E., Wilson, D.S., 2012. The Neogene period. *Geologic Time Scale 2012* (1–2), 923–978. <https://doi.org/10.1016/B978-0-444-59425-9.00029-9>.
- Ivanov, D., Ashraf, A.R., Mosbrugger, V., Palamarev, E., 2002. Palynological evidence for Miocene climate change in the Forecarpathian Basin (Central Paratethys, NW Bulgaria). *Palaeogeogr. Palaeoclimatol. Palaeoecol.* 178, 19–37.
- Ivanov, D., Utescher, T., Mosbrugger, V., Syabryaj, S., Djordjević-Milutinović, D., Molchanoff, S., 2011. Miocene vegetation and climate dynamics in Eastern and Central Paratethys (Southeastern Europe). *Palaeogeogr. Palaeoclimatol. Palaeoecol.* 304, 262–275.
- Kim, J.H., van der Meer, J., Schouten, S., Helmke, P., Willmot, V., Sangiorgi, F., Koç, N., Hopmans, E.C., Sinninghe Damsté, J.S., 2010. New indices and calibrations derived from the distribution of crenarchaeal isoprenoid tetraether lipids: Implications for past sea surface temperature reconstructions. *Geochim. Cosmochim. Acta* 74, 4639–4654.
- Kojumdzieva, E., Popov, N., 1988. Paléogéographie et evolution géodynamique de la Bulgarie Septentrionale au Néogène. *Geologica Balcanica* 19 (1), 73–92.
- Krijgsman, W., Stoica, M., Hoyle, T., Jorissen, E.L., Lazarev, S., Rausch, L., Bista, D., Alcicek, M.C., Ilgar, A., van den Hoek Ostende, L.W., Mayda, S., Raffi, I., Flecker, R., Mandic, O., Neubauer, T.A., Wesselingh, F.P., 2020. The myth of the Messinian Dardanelles: late Miocene stratigraphy and palaeogeography of the ancient Aegean-Black Sea gateway. *Palaeogeogr. Palaeoclimatol. Palaeoecol.* 560, 110033.
- Mosbrugger, V., Utescher, T., Dilcher, D.L., 2005. Cenozoic continental climatic evolution of Central Europe. *Proc. Natl. Acad. Sci.* 102, 42. [www.pnas.org/doi/10.1073/pnas.0505267102](http://www.pnas.org/doi/10.1073/pnas.0505267102).
- Niedermeyer, E.M., Forrest, M., Beckmann, B., Sessions, A.L., Mulch, A., Schefuß, E., 2016. *Geochim. Cosmochim. Acta* 184, 55–70.
- Ogg, J., 2020. Geomagnetic polarity time scale. In: Gradstein, F.M., et al. (Eds.), *Geologic Time Scale 2020*, pp. 159–192 (Elsevier, 2020). <https://doi.org/10.1016/B978-0-12-824360-2.00005-X>.
- Pagani, M., Arthur, M.A., Freeman, K.H., 1999. Miocene evolution of atmospheric carbon dioxide. *Paleoceanography* 14 (3), 273–292.
- Pagani, M., Pedentchouk, N., Huber, M., Sluijs, A., Schouten, S., Brinkhuis, H., Sinninghe Damsté, J.S., Dickens, G.R., Expedition 302 Scientists, 2006. Arctic hydrology during global warming at the Paleocene/Eocene thermal maximum. *Nature* 442, 671–675.
- Palcu, D.V., Golovina, L.A., Vernyhorova, Y.V., Popov, S.V., Krijgsman, W., 2017. Middle Miocene paleoenvironmental crises in Central Eurasia caused by changes in marine gateway configuration. *Glob. Planet. Chang.* 158, 57–71.
- Palcu, D.V., Vasiliev, I., Stoica, M., Krijgsman, W., 2019. The end of the Great Khersonian Drying of Eurasia: Magnetostatigraphic dating of the Maeotian transgression in the Eastern Paratethys. *Basin Res.* 31, 33–58.
- Palcu, D.V., Patina, I.S., Şandric, I., Lazarev, S., Vasiliev, I., Stoica, M., Krijgsman, W., 2021. Late Miocene megalake regressions in Eurasia. *Sci. Rep.* 11, 11471. <https://doi.org/10.1038/s41598-021-91001-z>.
- Peterse, F., van der Meer, J., Schouten, S., Weijers, J.W.H., Fierer, N., Jaccson, R.B., Kim, J.-H., Sinninghe Damsté, J.S., 2012. Revised calibration of the MBT-CBT paleotemperature proxy based on branched tetraether membrane lipids in surface soils. *Geochim. Cosmochim. Acta* 96, 215–229.
- Polissar, P.J., Freeman, K.H., 2010. Effects of aridity and vegetation on plant-wax dD in modern lake sediments. *Geochimica et Cosmochimica Acta* 74, 5785–5797.
- Popov, S.V., Shcherba, I.G., Iluina, L.B., Nevesskaya, L.A., Paramonova, N.P., Khondkarian, S.O., Magyar, I., 2006. Late Miocene paleogeography of the Paratethys and its relation to the Mediterranean. *Palaeogeogr. Palaeoclimatol. Palaeoecol.* 238, 91–106.
- Popov, S.V., Rostovtseva, Y.V., Gillipova, N.Y., Golovina, L.A., Radionova, E.P., Goncharova, I.A., Vernyhorova, Y.V., Dykan, N.I., Pinchuk, T.N., Iljina, L.B., Koromylova, A.V., Kocyrenko, T.M., Nikolaeva, I.A., Viskova, L.A., 2016. Paleontology and stratigraphy of the Middle-Upper Miocene of the Taman Peninsula. *Paleontol. J.* 50 (10), 1–168.
- Popp, B.N., Laws, E.A., Dore, J., Hanson, K.L., Wakeham, S.G., 1998. Effect of phytoplankton cell geometry on carbon isotopic fractionation. *Geochim. Cosmochim. Acta* 62 (1), 69–77.
- Ramstein, G., Fluteau, F., Besse, J., Joussaume, S., 1997. Effect of orogeny, plate motion and land-sea distribution on Eurasian climate change over the past 30 million years. *Nature* 386, 788–795.
- Razumkova, E.S., 2012. Palynological Characterization of the Sarmatian Deposits of the Eastern Paratethys (Section Zelenskiy Mountain–Panagiya, Taman Peninsula). *Stratigr. Geol. Correl.* 20 (1), 97–108.
- Sachse, D., Radke, J., Gleixner, G., 2004. Hydrogen isotope ratio of recent lacustrine sedimentary *n*-alkanes record modern climate variability. *Geochim. Cosmochim. Acta* 68, 4877–4889.
- Sant, K., Palcu, D.V., Mandic, O., Krijgsman, W., 2017. Changing seas in the Early-Middle Miocene of Central Europe: a Mediterranean approach to Paratethyan stratigraphy. *Terra Nova* 29, 273–281.
- Schouten, S., Hopmans, E.C., Schefuß, E., Sinninghe Damsté, J.S., 2002. Distributional variations in marine crenarchaeotal membrane lipids: a new tool for reconstructing ancient sea water temperatures? *Earth Planet. Sci. Lett.* 204, 265–274.
- Strömberg, C.A.E., Werdelin, L., Friis, E.M., Saraç, G., 2007. The spread of grass-dominated habitats in Turkey and surrounding areas during the Cenozoic: Phytolith evidence. *Palaeogeogr. Palaeoclimatol. Palaeoecol.* 250, 18–49.
- Syabryaj, S., Utescher, T., Molchanoff, S., Bruch, A., 2007. Vegetation and palaeoclimate in the Miocene of Ukraine. *Palaeogeogr. Palaeoclimatol. Palaeoecol.* 253, 153–168.
- Tzanova, A., Herbert, T.D., Pererson, L., 2015. Cooling Mediterranean Sea surface temperatures during the late Miocene provide a climate context for evolutionary transitions in Africa and Eurasia. *Earth Planet. Sci. Lett.* 419, 71–80.
- Van Dam, J.A., 1997. *Geol. Ultraiect.* 156.
- van der Meer, M.T.J., Sangiorgi, F., Baas, M., Brinkhuis, H., Sinninghe Damsté, J.S., Schouten, S., 2008. Molecular isotopic and dinoflagellate evidence for late Holocene freshening of the Black Sea. *Earth Planet. Sci. Lett.* 267, 426–434.
- Vasiliev, I., Reichart, G.J., Krijgsman, W., 2013. Impact of the Messinian Salinity Crisis on Black Sea hydrology—insights from hydrogen isotopes analysis on biomarkers. *Earth Planet. Sci. Lett.* 362, 272–282.
- Vasiliev, I., Reichart, G.J., Grothe, A., Sinninghe Damsté, J., Krijgsman, W., Sangiorgi, F., Weijers, J.W.H., van Roij, L., 2015. Recurrent phases of drought in the upper Miocene of the Black Sea region. *Palaeogeogr. Palaeoclimatol. Palaeoecol.* 423, 18–31.
- Vasiliev, I., Mezger, E.M., Lugli, S., Reichart, G.J., Manzi, V., Roveri, M., 2017. How dry was the Mediterranean during the Messinian salinity crisis? *Palaeogeogr. Palaeoclimatol. Palaeoecol.* 471, 120–133.
- Vasiliev, I., Reichart, G.J., Krijgsman, W., Mulch, A., 2019. Black Sea rivers capture drastic change in catchment-wide mean annual temperature and soil pH during the Miocene-to-Pliocene transition. *Glob. Planet. Chang.* 172, 428–439.
- Vasiliev, I., Feurdean, A., Reichart, G.J., Mulch, A., 2020. Late Miocene intensification of continentality in the Black Sea Region. *Int. J. Earth Sci.* 109, 831–846.
- Wang, W.-M., 2004. On the origin and development of Artemisia (Asteraceae) in the geological past. *Bot. J. Linn. Soc.* 145, 331–336.
- Weijers, J.W.H., Schouten, S., van der Donker, J., Hopmans, E.C., Sinninghe Damsté, J., 2007. Environmental controls on bacterial tetraether membrane lipid distribution in soils. *Geochim. Cosmochim. Acta* 71, 703–713.
- Weiss, G., Schouten, S., Sinninghe-Damsté, J.S., van der Meer, M.T.J., 2019. Constraining the application of hydrogen isotopic composition of alkenones as a salinity proxy using marine surface sediments. *Geochim. Cosmochim. Acta* 250, 34–48.
- Wessels, W., 2009. Miocene rodent evolution and migration. Muroidea from Pakistan, Turkey and Northern Africa. *Geol. Ultraiect.* 307, 1–290.